2014-07-15

Rapid prototyping amphiphilic polymer/hydroxyapatite composite scaffolds with hydration-induced self-fixation behavior

Artem B. Kutikov
University of Massachusetts Medical School

Et al.

TISSUE ENGINEERING: Part C
Volume 00, Number 00, 2014

DOI: 10.1089/ten.tec.2014.0213

Rapid Prototyping Amphiphilic Polymer/Hydroxyapatite Composite Scaffolds with Hydration-Induced Self-Fixation Behavior

Artem B. Kutikov, BS,[1,2] Anvesh Gurijala,[1] and Jie Song, PhD[1,2]

Two major factors hampering the broad use of rapid prototyped biomaterials for tissue engineering applications are the requirement for custom-designed or expensive research-grade three-dimensional (3D) printers and the limited selection of suitable thermoplastic biomaterials exhibiting physical characteristics desired for facile surgical handling and biological properties encouraging tissue integration. Properly designed thermoplastic biodegradable amphiphilic polymers can exhibit hydration-dependent hydrophilicity changes and stiffening behavior, which may be exploited to facilitate the surgical delivery/self-fixation of the scaffold within a physiological tissue environment. Compared to conventional hydrophobic polyesters, they also present significant advantages in blending with hydrophilic osteoconductive minerals with improved interfacial adhesion for bone tissue engineering applications. Here, we demonstrated the excellent blending of biodegradable, amphiphilic poly(D,L-lactic acid)-poly(ethylene glycol)-poly(D,L-lactic acid) (PLA-PEG-PLA) (PELA) triblock co-polymer with hydroxyapatite (HA) and the fabrication of high-quality rapid prototyped 3D macroporous composite scaffolds using an unmodified consumer-grade 3D printer. The rapid prototyped HA-PELA composite scaffolds and the PELA control (without HA) swelled (66% and 44% volume increases, respectively) and stiffened (1.38-fold and 4-fold increases in compressive modulus, respectively) in water. To test the hypothesis that the hydration-induced physical changes can translate into self-fixation properties of the scaffolds within a confined defect, a straightforward *in vitro* pull-out test was designed to quantify the peak force required to dislodge these scaffolds from a simulated cylindrical defect at dry versus wet states. Consistent with our hypothesis, the peak fixation force measured for the PELA and HA-PELA scaffolds increased 6-fold and 15-fold upon hydration, respectively. Furthermore, we showed that the low-fouling 3D PELA inhibited the attachment of NIH3T3 fibroblasts or bone marrow stromal cells while the HA-PELA readily supported cellular attachment and osteogenic differentiation. Finally, we demonstrated the feasibility of rapid prototyping biphasic PELA/HA-PELA scaffolds for potential guided bone regeneration where an osteoconductive scaffold interior encouraging osteointegration and a nonadhesive surface discouraging fibrous tissue encapsulation is desired. This work demonstrated that by combining facile and readily translatable rapid prototyping approaches with unique biomaterial designs, biodegradable composite scaffolds with well-controlled macroporosities, spatially defined biological microenvironment, and useful handling characteristics can be developed.

Introduction

Bone tissue engineering approaches aim to overcome the limitations of autografts (donor site morbidity and limited quantity) and allografts (high failure rate and risk for infections) for the repair of critical-size bone defects.[1] Tissue engineering typically employs degradable biomaterial scaffolds to support the delivery of cells/therapeutics to the defect site to guide/promote tissue regeneration and eventually be replaced by the regenerated tissue of interest.[2] The performance of such scaffolds is dependent not only on the chemical and structural properties of the biomaterial (e.g., chemical composition, network structure, and interfacial adhesion in the case of composites), but also the physical design (e.g., scaffold architecture and porosity), biological performance (e.g., osteoconductivity), and handling characteristics of the scaffold. Rational design that takes into consideration all of these factors is more likely to produce scaffolds that could meet clinical needs and are readily translatable (scalable and off-the-shelf).

Departments of [1]Orthopedics & Physical Rehabilitation and [2]Cell & Developmental Biology, University of Massachusetts Medical School, Worcester, Massachusetts.

The bioactivity of synthetic polymeric materials for orthopedic applications can be improved by structurally incorporating calcium apatite minerals such as hydroxyapatite (HA), the principle mineral component in bone. Besides the intrinsic osteoconductivity of HA[3] that encourages osteoblast/progenitor cell recruitment and growth,[4] the unique pH-dependent surface potential of HA also translates into the ability to enrich a wide range of endogenous protein factors and deliver exogenous protein therapeutics including osteogenic growth factors.[5,6] For polymer/HA composite materials, adequate interfacial adhesion between the polymer and mineral components is essential for achieving robust handling characteristics and mechanical properties.[7–9] However, most biodegradable polymers used to fabricate resorbable scaffolds are hydrophobic. This hydrophobicity/hydrophilicity mismatch results in poor interfacial adhesion and brittle composites with poor handling characteristics (i.e., difficulty to be press-fit into defects and prone to brittle fractures). Furthermore, hydrophobic materials cause difficulty in loading aqueous solutions (cells and/or growth factors) into the scaffold and may potentially change protein conformations via hydrophobic interactions, resulting in compromised bioactivity of the absorbed protein therapeutics.[10,11]

With the aim of developing an improved biodegradable polymer/HA composite, we recently reported a biodegradable amphiphilic block co-polymer, poly(D,L-lactic acid)-poly(ethylene glycol)-poly(D,L-lactic acid) (PLA-PEG-PLA) (PELA)-based HA composite.[12] By blending PELA with HA and electrospinning the stable suspension, we produced nonwoven fibrous meshes with more uniform morphologies, increased elasticity, and enhanced osteoconductivity and osteoinductivity when compared to electrospun HA-PLA composites. Interestingly, we also discovered that the amphiphilic nature of the electrospun scaffolds translated into superhydrophilicity (water contact angle $\sim 0°$) and an increased elastic modulus upon hydration. While electrospun HA-PELA would find unique orthopedic applications (e.g., as synthetic periosteal membrane wrapped around structural allografts), their limited thickness and porosity[13–15] make them less suited for treating large defects where sufficient nutrient transport and cellular ingrowth throughout a three-dimensional (3D) macroporous scaffold is desired.

Rapid prototyping techniques such as selective laser sintering,[16] powder-based 3D printing,[17] and fused deposition modeling (FDM) have been employed in the fabrication of large 3D scaffolds for bone tissue engineering. These rapid prototyping approaches have typically required custom-designed or expensive ($>$\$100,000) research-grade printers, limiting their widespread uses by the research community. Nevertheless, such techniques enable the formation of HA or HA/polymer composite scaffolds with defined geometries and controlled interconnected pore architecture. This scaffold design enables more homogenous cell distribution and ensures consistent mechanical properties that are not attainable by less-controlled fabrication techniques such as salt leaching or gas foaming.[18,19] While rapid prototyping technology has become increasingly refined, the selection of biomaterials suitable for prototyping has remained limited. The most widely prototyped polymers are hydrophobic polyesters such as poly(ε-caprolactone),[20–24] poly(L-lactic acid),[25] or poly(lactic acid-co-glycol acid).[26] Rapid prototyped amphiphilic polymer scaffolds composed of polyethyleneoxide-terephthalate (PEOT) and polybutylene-terephthelate (PBT) (PEOT/PBT) using a specialized printer have been explored for cartilage tissue engineering.[27–29] However, the PBT component is not biodegradable, resulting in crystalline, hard-to-resorb remnants upon degradations *in vivo*.[30] Furthermore, rapid prototyping HA-PEOT/PBT composite scaffolds for bone tissue engineering was not explored. We hypothesize that rapid prototyping HA-PELA scaffolds offers a unique opportunity to combine outstanding biological properties (osteoconductivity and osteoinductivity) of HA-PELA with a well-defined 3D macroporous architecture. Furthermore, we expect that the 3D HA-PELA scaffold would exhibit novel self-fixation behavior derived from the unique hydration-induced swelling and stiffening behavior of the amphiphilic composite.

Here, we report the rapid prototyping of interconnected macroporous PELA and HA-PELA scaffolds using an unmodified consumer-grade 3D printer. We examined the swelling behavior and mechanical properties of the scaffolds. We also quantitatively evaluated the hydration-induced self-fixation (as a result of hydration-induced swelling and stiffening) of the scaffolds using a custom-designed *in vitro* pull-out test employing a sample holder simulating a confined tissue defect. To demonstrate the utility of the 3D HA-PELA and PELA scaffolds for applications where opposing cell adhesive properties are desired (e.g., guided bone regeneration [GBR]),[31] we examined their respective ability to support the attachment and proliferation of NIH3T3 fibroblasts. For potential bone tissue engineering applications, we examined the attachment and osteogenic differentiation of rat bone marrow stromal cells (rMSCs) on HA-PELA. Finally, we demonstrated the feasibility of fabricating biphasic HA-PELA/PELA scaffolds by rapid prototyping using this consumer-grade 3D printer.

Materials and Methods

Materials

3,6-Dimethyl-1,4-dioxane-2,5-dione (D,L-lactide) was purchased from Sigma-Aldrich, purified by recrystallization twice in anhydrous toluene, and dried under vacuum prior to use. PEG (20,000 Da; BioUltra) was purchased from Fluka. Polycrystalline hydroxyapatite powder (consisting of loose aggregates of $\sim$100-nm crystallites) was purchased from Alfa Aesar. All other solvents and reagents were purchased from Sigma-Aldrich and used as received.

Polymer synthesis

PELA tri-block copolymer was synthesized and characterized as previously described.[12] Briefly, melt ring opening polymerization of D,L-lactide (0.12 mol) was initiated by PEG (20,000 Da, 0.2 mmol) with Tin(II) 2-ethylhexanoate ($\sim$95%, 0.06 mmol) catalysis. The reaction proceeded at 130°C for 5 h under argon. The crude PELA was dissolved in chloroform, purified by precipitation in methanol, and dried under vacuum before being subjected to gel permeation chromatography (GPC) characterizations (described in Scaffold Characterization section).

Scaffold fabrication

The manufacturing process for 3D PELA, HA-PELA, and PELA/HA-PELA biphasic scaffolds is depicted in Figure 1.

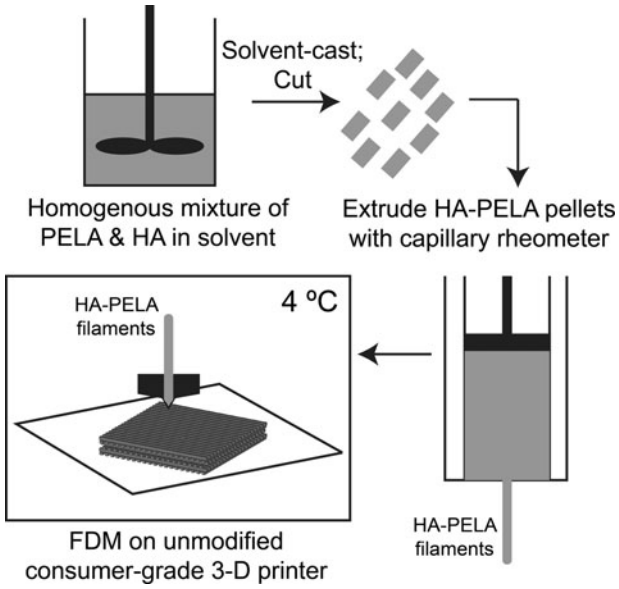

FIG. 1. Depiction of the preparation of PELA and HA-PELA three-dimensional (3D) scaffolds by rapid prototyping. HA, hydroxyapatite, PELA, poly(D,L-lactic acid)-poly(ethylene glycol)-poly(D,L-lactic acid).

Briefly, PELA/HA blends were solvent cast into films, extruded into filaments through a capillary rheometer, and then rapid prototyped into 3D scaffolds by FDM in a sub-ambient printing environment.

Preparation of PELA and HA-PELA films. PELA and HA-PELA dense films ($\sim$1.6 mm thick) were produced by solvent casting and sectioned into $\sim 0.5 \times 0.5\,cm^2$ pellets for filament extrusion. For the fabrication of HA-PELA composite films, HA (3.3 g, 25% w/w PELA) was bath-sonicated in 20 mL chloroform for 30 min. PELA (10 g) was added and the mixture was stirred overnight. The HA-PELA mixture was subsequently poured into Teflon molds. The chloroform was evaporated in a fume hood at room temperature overnight and subsequently in a vacuum oven at 60°C for 24 h. PELA films were prepared by evaporating a chloroform solution of PELA without HA in the same mold followed by vacuum drying under identical conditions.

Filament extrusion. The PELA and HA-PELA filaments were extruded using a LCR7000 capillary rheometer (Dynisco Instruments) through a 2.81-mm diameter die. The barrel was preheated at 130°C (for PELA) or 140°C (for HA-PELA) for $\sim$90 s before the PELA or HA-PELA pellets were loaded, followed by continued heating at the respective temperatures for 120 s. The filaments were extruded through the die with a 120-s run time and a barrel piston speed of 32.84-mm/min and collected manually.

Three-dimensional scaffold fabrication. A 3D computer-aided design (CAD) model of a 16×16 mm square prism (Fig. 2A, 2.4 or 4 mm in height) was designed in 3-Matics (Materialise) and converted into g-code instructions by MakerWare (MakerBot Industries). A MakerBot® Replicator™ 2X 3D printer (MakerBot Industries) cooled in a deli refrigerator at 4°C was used to print the scaffolds using the PELA or HA-PELA filaments. The sub-ambient printing environment was required to cool PELA below its T_g ($\sim$19°C) so that the filament could be continuously fed into the printer without undesired softening before reaching the heated printing nozzle. Nozzle temperatures of 130°C and 160°C were applied to print the PELA and HA-PELA, respectively. The build platform was maintained at 30°C to ensure stable adhesion of the bottom printed layer to the platform. Scaffolds were printed with a platform feed rate of 90 mm/s.

Biphasic PELA/HA-PELA scaffolds were fabricated by extruding three layers of HA-PELA followed by three layers of PELA. PELA and HA-PELA filaments were loaded into separate nozzles of the Replicator™ 2X. The same printing conditions described above for printing PELA and HA-PELA were applied accordingly.

Gel permeation chromatography

PELA and HA-PELA composites were dissolved in tetrahydrofuran (THF), centrifuged (720 *g*, 5 min) to pellet the HA, before the supernatant was collected and filtered with a 0.4-μm Teflon filter for GPC analyses. Molecular weights and polydispersity of PELA was determined by GPC on a Varian Prostar HPLC system equipped with two 5-mm PLGel MiniMIX-D columns (Agilent) and a PL-ELS2100 evaporative light scattering detector (Polymer Laboratories). THF was used as an eluent at 0.3 mL/h at room temperature. Molecular weight and polydispersity calculations were calibrated with EasiVial polystyrene standards (Agilent).

Scaffold characterization

Optical imaging. Macroscopic optical images of the HA-PELA, PELA, and the biphasic scaffolds were taken on a Leica M50 stereomicroscope equipped with a Leica DFC295 digital camera (Leica Microsystems).

Scanning electron microscopy and associated energy-dispersive X-ray spectroscopy. HA-PELA, PELA, and PELA/HA-PELA biphasic scaffolds were coated with 3 nm of carbon and imaged on a Quanta 200 FEG MKII scanning electron microscope (FEI, Inc.) under high vacuum at 10 kV. Energy-dispersive X-ray spectroscopy (EDX) was carried out to map the elemental compositions (calcium and phosphate [Ca and P]) of the biphasic scaffold at 15 kV with an Oxford-Link INCA 350 X-ray spectrometer (Oxford Instruments).

Porosity calculation. The theoretical porosity (P) of the scaffolds was calculated by determining the percentage (%) of scaffold volume that is occupied by the polymer rods, as described by Zein *et al.*[32] and shown in equation (1):

$$P = \frac{Va - Vt}{Va} \times 100\% \quad (1)$$

where Va (mm^3) is the apparent scaffold volume and Vt is the scaffold true volume taken up by polymer. Assuming that the FDM polymer rods are cylindrical in shape with a uniform diameter, the true volume taken up by polymer (Vt) in a square prism can be calculated as

$$Vt = L \times N \times Vrw \quad (2)$$

where L is the number of rods per layer, N is the number of layers, and Vrw is the volume of each cylindrical rod, which is determined by the printed line width and length.

Swelling behavior

The height and diameter (averaged from three measurements) of dry PELA and HA-PELA scaffolds ($n=3$), cored from the square prism FDM blocks using a biopsy punch, was measured with a digital caliper. Line width was averaged from five measured lines per scaffold using a light microscope (Axioscop 2 MAT; Carl Zeiss) and ImageJ (National Institutes of Health, Bethesda, MD). Scaffold mass was weighed using an analytical balance (ML104; Mettler-Toledo). Hydrated scaffold dimensions and mass were measured at various time intervals following incubation in deionized water at 37°C. Residual water was removed prior to weighing by briefly blotting the scaffolds on KimWipes. Change in mass (M/M_0) was calculated by dividing the mass following water equilibration (M) by the initial mass of a scaffold briefly submerged in water (M_0). Change in volume (V/V_0) was calculated in the same manner. Hydrated line width was measured following 24-h incubation in 37°C deionized water.

Mechanical testing

The compressive modulus of PELA and HA-PELA scaffolds ($n=3$) was determined on a Q800 DMA equipped with a liquid nitrogen gas cooling accessory (TA Instruments). Cylindrical specimens 6 mm in diameter and 4 mm in height, the dimensions used by Moroni *et al.* for characterizing mechanical properties of macroporous scaffolds,[19] were cored from the square prism FDM blocks. Unconfined compressive testing ($n=3$) was performed at 37°C for both dry (as-printed) and hydrated (24 h in deionized water) scaffolds. The height and diameter of each specimen was measured with a digital caliper prior to testing. Each specimen was held isothermal at 37°C for 30 min before being preloaded with a force of 0.001 N and ramped at a rate of 1.0 N/min to 10 N. The compressive modulus was recorded as the slope of the linear region (0–0.5% strain) of the stress/strain curve.

Pull-out test

A custom sample holder (Fig. 5A) simulating a confined circular tissue defect was developed to enable quantitative measurement of the hydration-induced self-fixation of the scaffolds via a pull-out test. A CAD model of the sample holder was designed in 3-Matics and fabricated on a MakerBot Thing-O-Matic™ 3D printer using acrylonitrile butadiene styrene (ABS). To ensure consistent specimen placement, the specimen holder portion of the ABS prototype was tight fitted with a standard cylindrical aluminum spacer (12.7 mm OD × 6.35 mm ID × 4.76 mm height; W.W. Grainger, Inc.). Cylindrical PELA or HA-PELA scaffolds 6 mm in diameter and 4 mm in height, cored from square prism FDM blocks using a biopsy punch, were each drilled with a center axial hole 1.6 mm in diameter to enable the insertion of a drywall nail (1.6 mm diameter, 32 mm long, 3.8 mm diameter head, Fig. 5B). The specimen was inserted into the aluminum spacer, and either tested dry or equilibrated in deionized water within the holder for 2 h at 37°C prior to test. The bottom stem of the custom ABS holder and the sharp end of the inserted nail were secured between the grips of a MTS Bionix 370 mechanical testing system (MTS Systems Corporation), respectively (Fig. 5C). Specimens were ramped at a rate of 50 mm/min until they are completely pulled out of the ABS/aluminum holder to determine the peak force as recorded by a 250 N load cell (Interface).

NIH3T3 cell attachment and proliferation

HA-PELA and PELA scaffolds (6.3 mm in diameter, 2.4 mm in height) were washed thrice in deionized water (5 min per wash), sterilized in 70% ethanol, and allowed to air dry in a laminar flow hood. Residual ethanol was removed with a wash in phosphate-buffered saline (PBS) followed by equilibration overnight in Dulbecco's modified Eagle's medium (DMEM, high glucose; Life Technologies) supplemented with 10% bovine calf serum and 1% penicillin/streptomycin. Immediately prior to cell seeding, media were removed from the scaffolds by vacuum and the scaffolds were transferred to ultra-low attachment 24-well plates (Corning, Inc.). NIH3T3 fibroblasts were trypsinized from adherent culture and seeded on the scaffolds (200,000 cells in 50 μL of media), and allowed to attach in an incubator (37°C, 5% CO_2) for 1 h.

A Cell Counting Kit-8 assay (CCK-8; Dojindo Molecular Technologies, Inc.) was performed to assess the viability of cells attached on the scaffolds. At each time point, cell-laden scaffolds were transferred to a fresh well containing 0.7 mL of media and 9% (v/v) CCK-8 reagent. After 4-h incubation, 100 μL of media was removed for measurement of absorbance at 450 nm with 650 nm background correction on a Multiskan FC microplate photometer (Thermo Scientific). The remainder of the media was aspirated, the scaffolds were washed with PBS, and replaced with fresh media for continued culture up to 14 days. The CCK-8 assay was carried out at day 1, 3, 5, 7, and 14.

NIH3T3 attachment on the HA-PELA and PELA scaffolds was also visualized by staining the viable cells with formazan dye using a MTT kit (Cell Proliferation Kit I; Roche). At 24 h postseeding, scaffolds were transferred to a fresh well containing media with 9% (v/v) MTT labeling reagent. After 3 h of incubation, the scaffolds were imaged on a Leica M50 stereomicroscope equipped with a Leica DFC295 digital camera (Leica Microsystems).

rMSC attachment and osteogenic differentiation

rMSCs were isolated from 289 to 300 g male Charles River SD rats according to the procedure approved by the University of Massachusetts Medical School Institutional Animal Care and Use Committee, and enriched by adherent culture as previously described.[33] The cells were cultured in MSC expansion media (αMEM without ascorbic acid, containing 20% fetal bovine serum, 1% penicillin–streptomycin, and 2% L-glutamine). Passage 3 MSCs were seeded onto the scaffolds (200,00 cells in 50 μL of media), and a CCK-8 assay was performed after 24 h as described in the previous section.

In a separate set of experiments, rMSCs were seeded onto the HA-PELA scaffolds (400,000 cells in 50 μL media) and allowed to attach in a humidified incubator (37°C, 5% CO_2) for 1 h. Following attachment, 0.7 mL of fresh expansion media were added and the scaffolds were cultured for 24 h. To induce osteogenic differentiation, the media then were replaced with MSC expansion media supplemented with

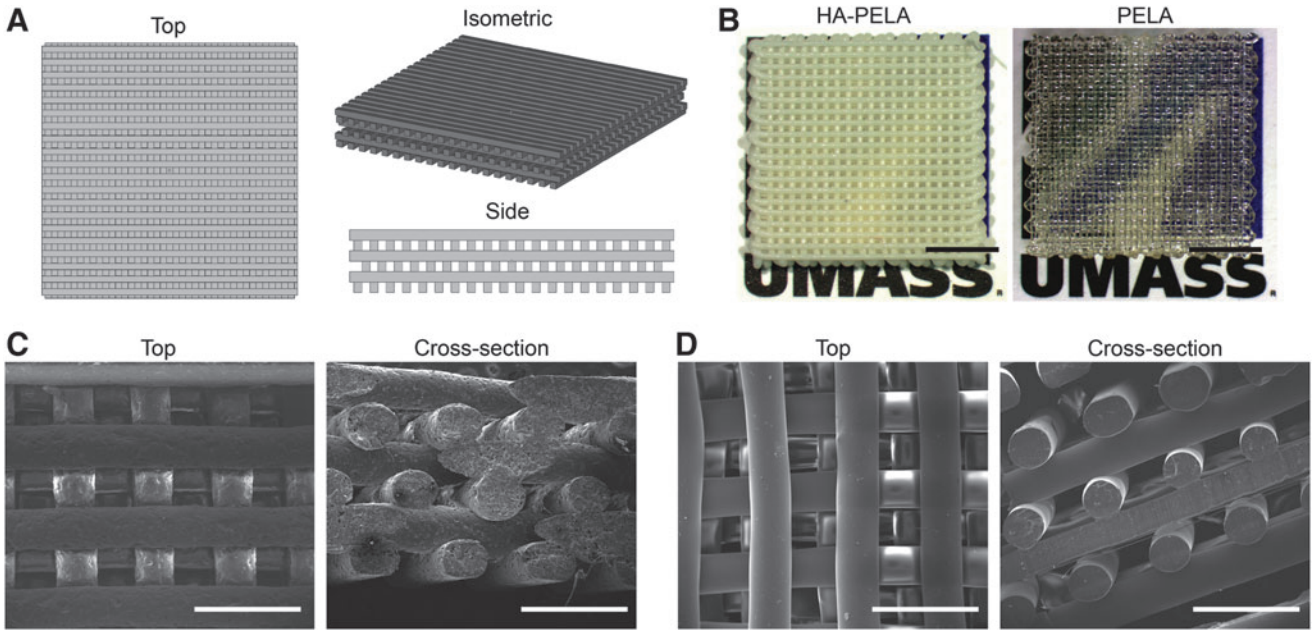

FIG. 2. **(A)** Top, isometric, and side views of scaffold CAD design. **(B)** Stereomicroscopy images of rapid prototyped HA-PELA and PELA scaffolds. Scale bars = 5 mm. **(C)** Scanning electron micrographs of the HA-PELA scaffold. Scale bars = 1 mm. **(D)** Scanning electron micrographs of the PELA scaffold. Scale bars = 1 mm. Color images available online at www.liebertpub.com/tec

10 nM of dexamethasone, 20 mM of β-glycerol phosphate, and 50 μM of L-ascorbic acid 2-phosphate. The scaffolds were cultured in either expansion or osteogenic media for 14 days with medium changes twice a week. Alkaline phosphatase staining was performed with an Alkaline Phosphatase Leukocyte kit according to manufacturer's instructions (Sigma-Aldrich). The protocol was modified to fix the scaffolds in 4% neutral buffered formalin for 15 min rather than in the citrate-acetone-formaldehyde fixative because the scaffolds are soluble in acetone. Alkaline phosphatase-stained scaffolds were imaged on a stereomicroscope.

For observation of the microscopic morphology of the adherent cells and the deposited extracellular matrices by scanning electron microscopy (SEM), the scaffolds were air dried, sputter coated with Au (~12 nm), and imaged on a Quanta 200 FEG MKII scanning electron microscope under high vacuum at 5 kV.

Statistical analysis

All data are presented as mean ± standard deviation. Statistical analysis was performed using ANOVA with Tukey *post hoc*.

Results

Fabrication and characterization of PELA and HA-PELA scaffolds

CAD software was used to design 16 × 16 mm square prism scaffolds with a staggered arrangement of lines (Fig. 2A). The line width and height was set to 0.4 mm, the same as the printing nozzle diameter. The perpendicular and staggered line arrangements between neighboring and alternating layers, respectively, were designed to maximize the retention of cells during initial cell seeding. Line spacing of 0.4 mm, which was shown to be advantageous over large spacing (e.g., 0.8 mm) in achieving sufficient seeding efficiency, was used to give a theoretical scaffold porosity of 61.7%. Six-layer (2.4 mm high) scaffolds were designed for all cell culture studies and 10-layer (4.0 mm high) scaffolds were designed for all physical characterizations. The scaffolds were rapid prototyped based on the CAD models by FDM on an unmodified consumer-grade 3D printer. Macroscopic images of the scaffolds (Fig. 2B) revealed that their line width was consistent with the CAD model (0.4 mm). Scanning electron micrographs showed a roughened fiber appearance for the HA-PELA composite scaffolds (Fig. 2C) while a smooth fiber appearance for the un-mineralized PELA scaffold (Fig. 2D). Cross sections of both scaffolds revealed circular fibers with open pores between fibers (Fig. 2C, D).

GPC was used to determine the effect of filament extrusion and rapid prototyping on the molecular weight and polydispersity of PELA (Table 1). PELA underwent a slight

Table 1. Molecular Weight Distribution during the Processing of PELA and HA-PELA

PELA sample	*Proc. temp.*[a]	M_n	M_w	M_n/M_w
As synthesized PELA		85,873	134,077	1.56
HA-PELA filament	140°C	84,615	129,902	1.53
HA-PELA scaffold	160°C	82,537	130,945	1.58
PELA filament	130°C	75,553	116,465	1.54
PELA scaffold	130°C	76,415	117,039	1.53

[a]Referring to the filament extrusion temperature or the nozzle temperature applied for prototyping the scaffolds.

HA, hydroxyapatite; PELA, poly(D,L-lactic acid)-poly(ethylene glycol)-poly(D,L-lactic acid).

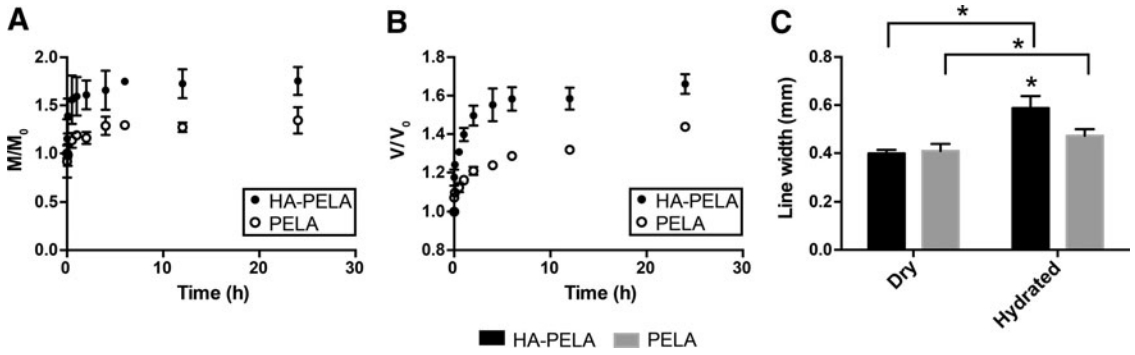

FIG. 3. Swelling behavior of HA-PELA and PELA scaffolds ($n=3$). **(A)** Change in scaffold mass (swelled mass [M]/initial mass [M_0]) over time in deionized water at 37°C. **(B)** Change in scaffold volume (swelled volume [V]/initial volume [V_0]) over time in deionized water at 37°C. **(C)** Change in line width after 24 h hydration in deionized water at 37°C ($*p<0.05$).

decrease in molecular weight, while the molecular weight of HA-PELA was minimally affected by the fiber extrusion at elevated temperatures (130°C for PELA and 140°C for HA-PELA). The rapid prototyping of PELA at the same nozzle temperature of 130°C, however, did not lead to further decreases in the molecular weight of the printed PELA scaffold. No significant changes in the molecular weight distributions of PELA and HA-PELA were detected throughout the extrusion and rapid prototyping.

Swelling behavior of HA-PELA and PELA

The swelling and water absorption behavior of the HA-PELA and PELA scaffolds ($n=3$) in deionized water at 37°C was monitored over time (Fig. 3). The mass and volume of HA-PELA scaffolds increased more rapidly than PELA, resulting in a higher total swelling after 24 h (Fig. 3A, B). The mass and volume of both scaffolds increased more rapidly within the first 2–4 h, followed by slower but continued increases, reaching 75% (mass) and 66% (volume) for HA-PELA, and 34% (mass) and 43.8% (volume) for PELA by 24 h, respectively. The line width of the scaffolds also increased over the 24 h swelling period for both scaffolds (Fig. 3C), with the fully hydrated HA-PELA scaffold exhibiting significantly higher line width than that of PELA.

Hydration-induced stiffening of the scaffolds

The effect of hydration on the compressive modulus of HA-PELA and PELA scaffolds was determined by unconfined compressive testing at 37°C. In both dry and hydrated states, HA-PELA exhibited a significantly higher compressive modulus than PELA (Fig. 4). After hydration in 37°C deionized water for 24 h, the compressive moduli of both HA-PELA and PELA significantly increased. The magnitude of hydration-induced stiffening was higher for PELA than HA-PELA, with an increase in compressive modulus of 395% compared to 37.5%.

Hydration-induced self-fixation of scaffolds in a simulated confined defect

A device was designed to assess how the hydration-induced swelling and stiffening of the HA-PELA and PELA scaffolds may be exploited to facilitate their stable self-fixation into skeletal tissue defects as synthetic bone grafts. The CAD model and rapid prototyped ABS testing device (Fig. 5A) incorporated a cylindrical aluminum spacer to hold a cylindrical test specimen. The specimen was secured to the grips of a MTS mechanical testing system by the bottom stem of the testing device and a drywall nail penetrating through the center axis of the specimen (Fig. 5B). This design allows convenient placement of a test specimen in a confined cylinder to allow for a pull-out test to be reproducibly carried out on any standard mechanical testing machine (Fig. 5C). The peak force required to pull the scaffold out of the specimen holder via the nail grip was determined. This force was measured for dry HA-PELA and PELA scaffolds and for scaffolds preswelled in the fixation device in deionized water at 37°C for 2 h. The peak force increased by 15-fold and 6.3-fold following hydration of HA-PELA and PELA scaffolds in the fixation device, respectively (Fig. 5D). The peak fixation force of the hydrated HA-PELA scaffolds was significantly higher than that of the hydrated PELA scaffolds. The observed increase in peak force upon hydration, positively correlated with the difficulty of pulling out the specimen, is a potential indicator of how the specimens may swell/stiffen and become stably fixated within a tissue defect.

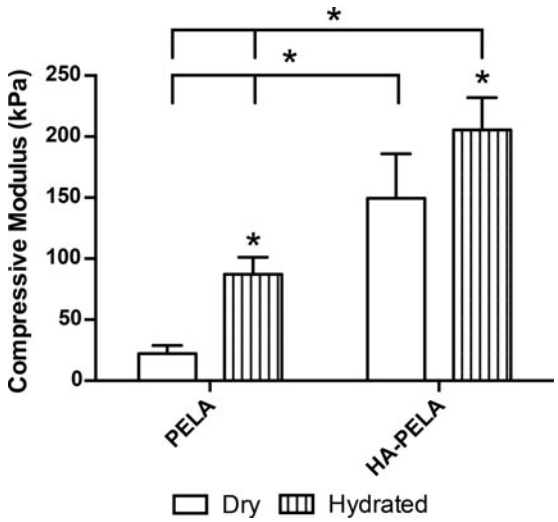

FIG. 4. Compressive moduli of dry and hydrated PELA and HA-PELA scaffolds ($n=3$) at 37°C ($*p<0.05$).

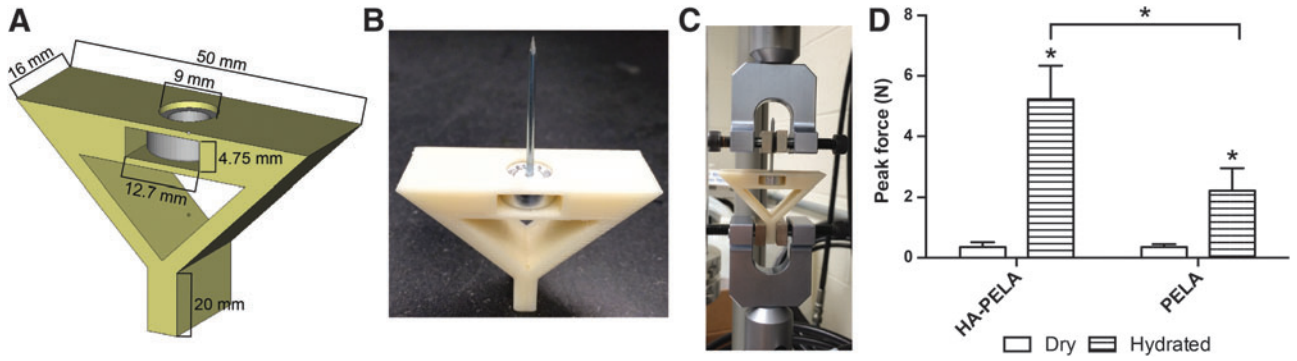

FIG. 5. Hydration-induced self-fixation test. **(A)** CAD image of the self-fixation testing device with aluminum spacer. **(B)** Image of the rapid prototyped self-fixation testing device with HA-PELA scaffold inserted. **(C)** Image of the testing device secured to the grips of the MTS mechanical testing system. **(D)** Peak forces required to pull HA-PELA and PELA scaffolds ($n=4$) out of the testing device before and after hydration ($^*p<0.05$). Color images available online at www.liebertpub.com/tec

NIH3T3 attachment and proliferation on the rapid prototyped scaffolds

A CCK-8 assay was used to quantify the viability of NIH3T3 fibroblasts cultured on HA-PELA and PELA scaffolds (Fig. 6A). The CCK-8 reagent has low toxicity and the colored formazan product is soluble in media, allowing the cellular viability on the same scaffolds to be longitudinally monitored in a nondestructive manner. Initial cell attachment was significantly higher on HA-PELA than PELA, and the much higher cellular viability was maintained on HA-PELA for 14 days. The extremely poor cellular attachment on PELA resulted in further cell death, leaving few viable cells on PELA by day 3. Differences in cell attachment between HA-PELA and PELA were further confirmed by staining viable cells with formazan dye (Fig. 6B). The HA-PELA scaffolds supported the attachment of viable cells evenly distributed across different layers of the composite scaffold. The PELA scaffold, however, only contained a small number of viable cells trapped within the pores, with few cells directly adhered to the low-fouling fibers.

MSC attachment and osteogenic differentiation on the rapid prototyped scaffolds

The MSC attachment on HA-PELA was assessed to determine the suitability of HA-PELA for supporting potential stem/progenitor cell attachment and bone in-growth *in vivo*.

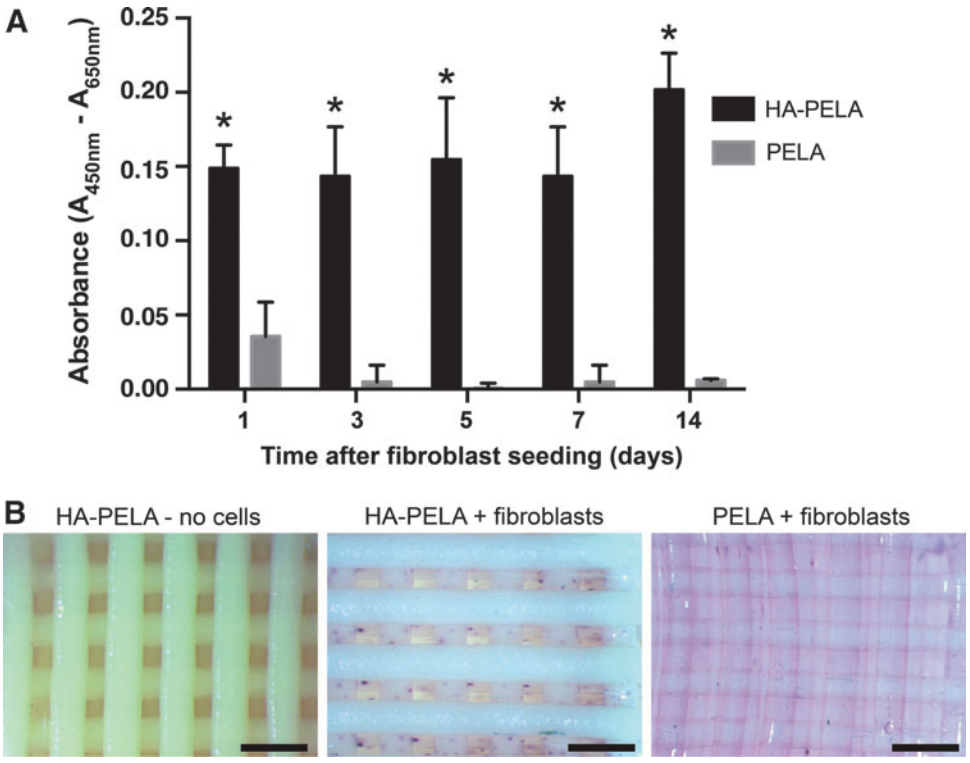

FIG. 6. **(A)** CCK-8 cell viability assay of NIH3T3 attachment and proliferation on HA-PELA and PELA scaffolds ($n=3$) ($^*p<0.05$). **(B)** Stereomicroscopy images of MTT stained scaffolds 24 h post-NIH3T3 seeding. *Dark purple* stains denote viable cells adhered on the scaffolds. Scale bars = 1 mm. Color images available online at www.liebertpub.com/tec

CCK-8 assay revealed significantly higher (e.g., 16-fold increase in viable cells at 24 h) seeding efficiency of MSCs on the 3D HA-PELA scaffolds than on the PELA scaffolds (Fig. 7A), further supporting the cell-adhesive nature/osteoconductivity of the former and the low-fouling nature of the latter. The ability of the HA-PELA scaffold to support osteogenic differentiation of rMSCs was examined by culturing the cells on the scaffolds in expansion or osteogenic media for 14 days. Extensive positive (red) alkaline phosphatase staining detected throughout the 3D macroporous scaffold (e.g., as revealed by surface, side and cross-section views) confirmed the osteogenic differentiation of the adherent rMSCs cultured in osteogenic media (Fig. 7B). No nonspecific staining was detected in the expansion media control. SEM micrographs revealed the deposition of extracellular matrices including mineral nodules surrounding the rMSCs adhered to the scaffold after the 14-day culture in osteogenic differentiation media (Fig. 7C), further confirming that these rMSCs underwent osteogenic differentiation upon culture induction.

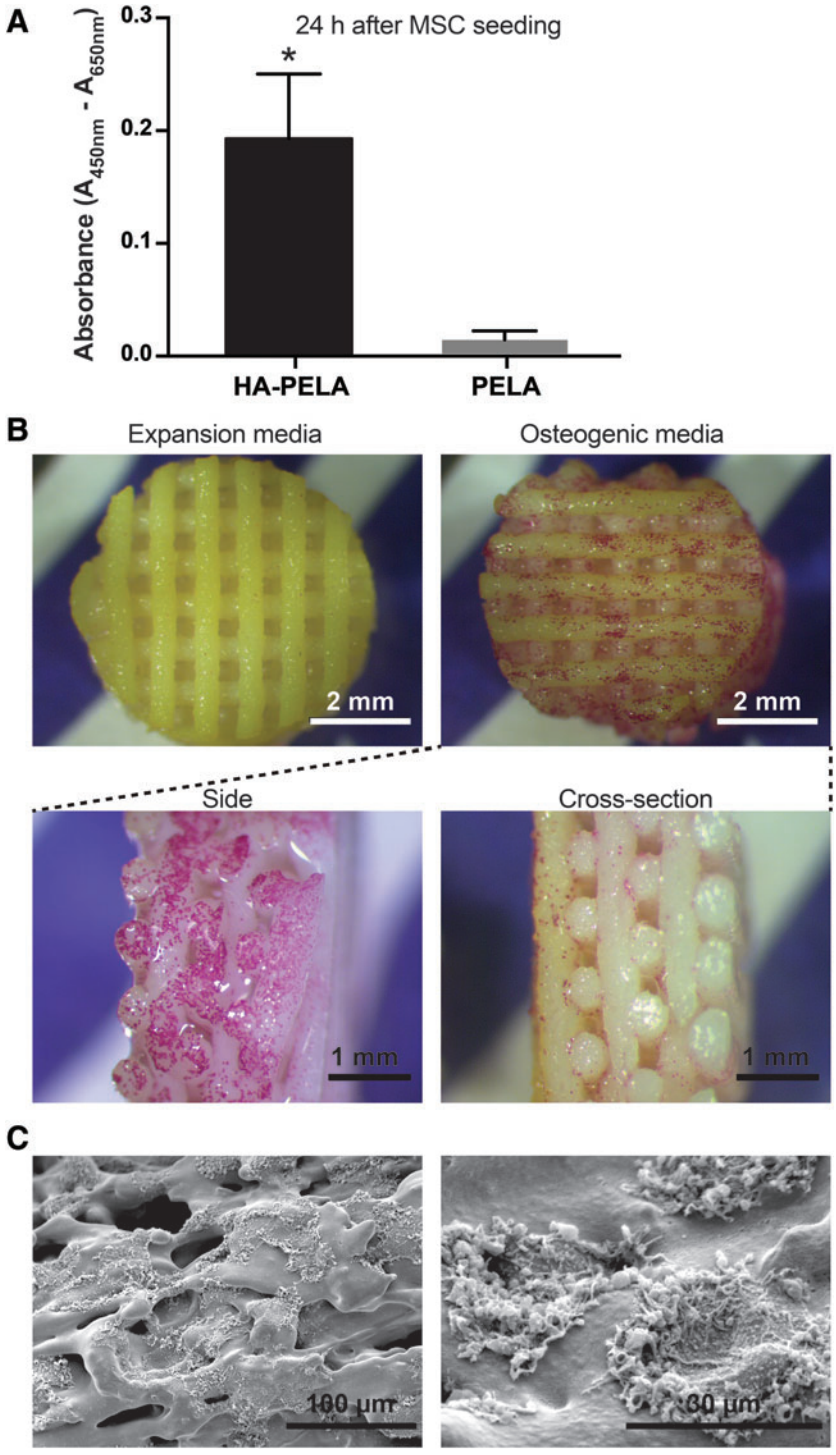

FIG. 7. rMSC attachment and osteogenic differentiation on HA-PELA scaffolds. **(A)** CCK-8 cell viability assay of rMSCs attached to HA-PELA and PELA scaffolds at 24 h after initial seeding ($n = 3$) ($^*p < 0.05$). **(B)** Alkaline phosphatase staining of rMSCs cultured on HA-PELA in expansion media (*left*) or osteogenic media (*right*) for 14 days. Side and cross-section views of the stained scaffold cultured in osteogenic media are shown below. **(C)** Scanning electron microscopy micrographs of rMSCs cultured on HA-PELA in osteogenic media for 14 days. rMSCs, rat bone marrow stromal cells. Color images available online at www.liebertpub.com/tec

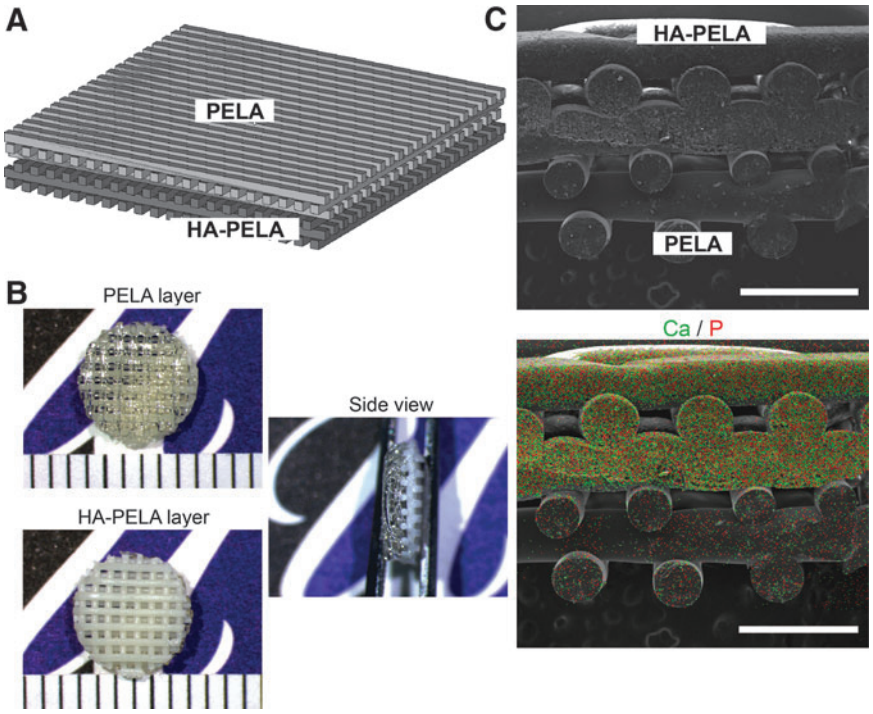

FIG. 8. PELA/HA-PELA biphasic scaffold. **(A)** CAD model of the PELA/HA-PELA biphasic scaffold. **(B)** Stereomicroscopy images of a 6-mm core punched out from the biphasic scaffold. Scale markings = 1.0 mm **(C)** Scanning electron micrograph of a biphasic scaffold (*top*). Elemental mapping overlay (*bottom*) of calcium (*green*) and phosphate (*red*). Scale bars = 1 mm. Color images available online at www.liebertpub.com/tec

Rapid prototyping biphasic PELA/HA-PELA scaffolds

Biphasic scaffolds composed of 3 PELA layers and 3 HA-PELA layers were designed using CAD (Fig. 8A) and fabricated by FDM. Stereomicroscopy images showed distinct yet well-connected PELA and HA-PELA phases (Fig. 8B). SEM and EDX mapping of the cross section of the biphasic scaffold confirmed the distinct mineral composition in the HA-PELA fibers (Fig. 8C). The calcium (Ca) and phosphate (P) signals were clearly localized within and on the surface of the HA-PELA fibers while only minor background noise was detected in the adjacent PELA phase.

Discussion

Recent work from our group has demonstrated the potential of electrospun HA-PELA scaffolds for bone tissue engineering applications.[12] Compared with hydrophobic PLA, amphiphilic PELA exhibited significantly improved mechanical properties (10-fold increase in ultimate tensile strain), hydrophilicity, and bioactivity (osteoconductivity and highly sensitized response of MSCs to osteogenic induction) when combined with HA.[12] Furthermore, the amphiphilic nature of PELA resulted in hydration-induced structural rearrangement (supported by differential scanning calorimetry) and stiffening of the polymers,[12] a property that we hypothesize could be exploited to create scaffolds that can secure themselves within a confined bony defect (self-fixation). Here, we demonstrated facile fabrication of 3D PELA, HA-PELA, and biphasic scaffolds with controlled macroporosity and architecture by FDM using a consumer-grade 3D printer. We evaluated their swelling and mechanical properties under physiological conditions and designed a fixation test to examine the ability of the scaffolds to self-fixate within a confined cylindrical defect upon hydration *in vitro*. Furthermore, we evaluated these scaffold's abilities to support cell adhesion/growth, thereby determining the suitability of the biphasic scaffold for applications such as GBR.

The FDM process consists of feeding a thermoplastic polymer filament through a heated nozzle, guided by software instructions converted from the CAD model, and depositing thin rods of polymer layer by layer that fuse with one another at their contact points. We used an unmodified consumer-grade 3D printer (MakerBot Replicator™ 2X) to fabricate the scaffolds. The only ''customization'' required for printing PELA and HA-PELA polymers are (1) the preparation of PELA and HA-PELA filaments to feed the 3D printer, and (2) the identification of appropriate environmental and printing nozzle temperatures to support the smooth feeding (without premature softening) and printing (without degradation) of PELA/HA-PELA rather than ABS, the default polymer used for the MakerBot Replicator™ 2X.

To produce the filaments for FDM, a capillary rheometer was used to extrude the PELA and HA-PELA. The capillary rheometer or melt flow indexer allowed for smaller quantities of polymer (gram-scale vs. kilogram-scale required by conventional extruder) to be used. The melt flow indexer is also more cost effective (< $5000) compared to microextruders (> $100,000). We extruded prefabricated dense films obtained from solvent casting where loose aggregates of HA nanocrystals[33] were homogeneously blended with PELA in the composite. To ensure that the filament was smoothly fed into the heated printing nozzle without premature softening, we carried out the FDM in a deli refrigerator at 4°C, well below the glass transition temperature of PELA (~19°C). This temperature prevented the filament from softening/melting and sticking in the drive gear before reaching the printing nozzle, the temperature of which was set at 130°C for PELA and 160°C for HA-PELA. With this approach, we were able to fabricate PELA and HA-PELA

scaffolds with fiber dimensions precisely matching the CAD model (Fig. 2) without undesired line width widening/thinning due to inconsistent extrusion through the heated nozzle. GPC confirmed that the printing nozzle temperature chosen largely maintained the integrity of PELA and HA-PELA composite (Table 1). It is worth noting that the molecular weight of the HA-PELA composite decreased less than the molecular weight of PELA during the filament extrusion and subsequent processing, even though the processing temperatures for HA-PELA were higher, suggesting an insulating and protective effect of HA on the degradable polymer. This result is consistent with our prior observation that the electrospun HA-PELA meshes exhibited an increased thermal decomposition temperature than the PELA meshes as determined by thermogravimetric analysis.[12]

PEG/PLA co-polymers are known to exhibit significant water absorption due to the hydrophilic PEG segment.[34,35] Additionally, we showed previously that electrospun PELA and HA-PELA meshes significantly stiffened upon hydration.[12] Here, we examined the swelling behavior and hydration-dependent mechanical properties of the rapid prototyped porous PELA and HA-PELA scaffolds at 37°C. Both HA-PELA and PELA 3D scaffolds were readily wetted by water and exhibited significant swelling in water within 2 h, with the prototyped line width increasing by 25% in 24 h (Fig. 3). The incorporation of HA significantly increased the swelling of the scaffolds. This result may be attributed to the further increased hydrophilicity upon HA incorporation and the more roughened HA-PELA fiber morphologies that promoted better water penetration within HA-PELA. These observations support that the 3D PELA-based scaffolds are highly hydrophilic, in agreement with prior water contact angle and swelling experiments carried out on electrospun PELA meshes and dense solvent-cast PELA films.[12,36]

Polymers typically soften upon hydration due to the plasticizing effect of water.[37] However, hydration-induced stiffening has been previously described for electrospun PELA[12] and other amphiphilic polymers.[37,38] This phenomenon is likely caused by hydration-induced phase separation of the hydrophilic PEG blocks from the hydrophobic segments,[12,37,39] which was confirmed by modulated differential scanning colorimetry with our electrospun PELA or HA-PELA fibrous meshes[12] and by small-angle X-ray scattering of other related amphiphilic systems.[37] We showed here that the compressive moduli of 3D HA-PELA were higher than those of the PELA scaffolds in both dry and hydrated states (Fig. 4). The hydration-induced increase in compressive modulus was observed with both scaffolds, but the effect was more pronounced in PELA ($\sim$4-fold increase) than in HA-PELA (1.38-fold increase). However, the fully hydrated HA-PELA scaffold was more than twice as stiff as the hydrated PELA scaffold. The higher (by 6.7-fold) modulus of the dry HA-PELA scaffold compared to the dry PELA supported good structural integration of HA with the amphiphilic polymer. The increase in stiffness of the hydrated HA-PELA suggests that HA did not disrupt the hydration-induced phase separation of PELA.

The swelling behavior and hydration-induced stiffening of the rapid prototyped amphiphilic scaffolds led us to hypothesize that a dry HA-PELA or PELA scaffold readily placed within a confined tissue defect (with minimal resistance) could gradually conform to the defect upon swelling under physiological conditions and remain securely fixed within the defect as it stiffens. Such a gradual self-fixation would allow both convenient placement and better integration of an implant within the often complex defect geometries. Inspired by push-out tests evaluating the fixation of osseous implants to surrounding native bone tissue,[40,41] we developed an *in vitro* pull-out test to quantify the hydration-induced self-fixation behavior. The test specimen was placed into a rapid prototyped testing device (Fig. 5B), allowed to swell in water, and the force required to pull it out of the testing device was measured. While this test does not fully recapitulate the environment of a tissue substrate, it provides a reproducible and facile method to quantitatively compare the self-fixation behavior of various scaffolds *in vitro,* thereby serving as a valuable, although imperfect, predictor. We observed significant fixation of both HA-PELA and PELA scaffolds after 2 h of hydration (Fig. 5D). The peak force required to remove the hydrated HA-PELA scaffold was 15-fold higher than that for the dry scaffold. The fixation force measured for the hydrated HA-PELA was also significantly higher than that of hydrated PELA, likely due to a combination of the more pronounced swelling and the more substantial stiffening of the hydrated HA-PELA. To our knowledge, this is the first report of rapid prototyped biomaterial scaffold exhibiting well-characterized hydration-induced self-fixation behavior.

The low-fouling PEG component in PEG-PLA di-block films[36,42,43] and electrospun PELA[44,45] was previously shown to translate into low cellular adhesion. In our prior work, we showed that the electrospun HA-PELA meshes, unlike the low-fouling PELA counterpart, readily supported cellular adhesion and proliferation of bone marrow-derived stromal cells.[12] The substantial difference between PELA and HA-PELA in supporting cell adhesion could potentially be exploited for applications where varying degrees of tissue ingrowth are required on opposing sides of a biomaterial scaffold. One such application is GBR.[31] The principle behind GBR is to exclude fibroblasts and soft tissue from occupying the bony defect while encouraging the defect to be populated with osteogenic cells and filled with new bone.[46,47] We hypothesized that the low-fouling PELA, when properly incorporated into the scaffolds, would inhibit this fibroblast adhesion. Using a CCK-8 assay, we showed that the PELA scaffold indeed restricted the adhesion of fibroblasts (Fig. 6A). Only a small number of fibroblasts loosely adhered to the PELA scaffold, as visualized by MTT staining after 24 h (Fig. 6B), and they failed to proliferate over time (Fig. 6B). By contrast, nearly 5 times fibroblasts adhered to the HA-PELA upon cell seeding and they remained viable and stably attached to the scaffold during the 14-day culture period (Fig. 6A, B), agreeing with the general trend we previously observed with electrospun PELA versus HA-PELA scaffolds.[12]

We further confirmed that the osteoconductive HA-PELA readily supported the cellular adhesion and differentiation of MSCs. The incorporation of HA effectively offset the low-fouling effect of the PEG component of the amphiphilic composite, resulting in 10 times higher rMSC seeding efficiency on HA-PELA than on the PELA (Fig. 7A). The rMSCs remained adhered over long-term culture (14 days) and were able to differentiate and produce mineralized extracellular matrix in the presence of osteogenic media (Fig. 7B, C). Combined with previously elucidated highly

sensitized response of the MSCs adhered to HA-PELA (as opposed to PELA or HA-PLA) to osteogenic inductions,[12] these observations support 3D HA-PELA as a promising scaffold for GBR upon surgical implantation to a bony defect. While this study did not attempt to optimize of scaffold porosity and architecture, new computational modeling methods such as those based on triply periodic minimal surfaces could be employed to enable CAD of macroporous scaffolds with further improved cell seeding efficiency and mechanical properties.[48–51] Chemical modification of PELA with reactive groups to support techniques such as projection stereolithography would facilitate the fabrication of such next-generation scaffold designs.[52]

As a proof of concept, we fabricated a PELA/HA-PELA biphasic scaffold for potential GBR applications using the consumer-grade 3D printing system (Fig. 8). The top low-fouling PELA phase was designed to prevent fibroblast adhesion/scar tissue encapsulation/soft tissue collapse into the defect *in vivo* while the bottom HA-PELA phase, upon insertion into a bony defect, was designed to support the attachment of osteoblasts or progenitors residing in the bony tissue environment to encourage bone ingrowth. Outstanding control in line width and clear separation of the distinct phases (Fig. 8B, C) was accomplished in the biphasic construct using the consumer-grade printer.

A PubMed search for prototyping publications in the past decade combining keyword search results from ''fused deposition modeling,'' ''three-dimensional printing,'' and ''rapid prototyping'' revealed an interesting trend indicative of the need for easier-to-use and more versatile rapid prototyping instrumentation to achieve broader and more sustained use of this technology (Fig. 9). The number of rapid prototyping-related publications appeared to have plateaued by 2010 with increasing numbers of publications in 2013. By comparison, the electrospinning technique, garnered initial attention from the research community almost 4 years later than rapid prototyping yet had seen a much more rapid and sustained growth in terms of related publications (e.g., resulting in twice as many publications in 2013). This discrepancy in the number of publications may be in part due to the substantially lower investment (e.g., a few thousand dollars) required for an electrospinning setup than for custom-designed or research-grade printing systems (e.g., could be >$100,000). With the popularization of consumer-grade printers in the past few years, the use of rapid prototyping technology for fabricating novel biomaterial scaffolds by research laboratories and biotech industries could see a renewed upward trend.

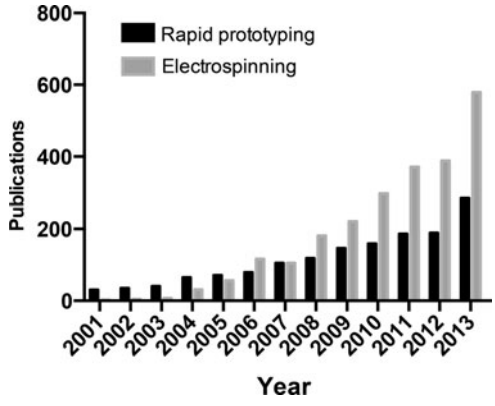

FIG. 9. Number of PubMed citations of rapid prototyping and electrospinning publications since 2001. Search results based on the key words ''rapid prototyping,'' ''fused deposition modeling,'' and ''three-dimensional printing'' were combined for the total rapid prototyping publications in each calendar year.

Conclusions

To the best of our knowledge, this study is the first to rapid prototype PELA or HA-PELA, a class of amphiphilic degradable biomaterials recently shown to exhibit exciting physical (e.g., hydrophilicity, mechanical integrity, and hydration-induced structural rearrangement and mechanical strengthening effect) and biological properties (e.g., osteoconductivity and upregulated osteogenic gene expression),[12] into 3D macroporous tissue engineering scaffolds. We describe the use of an unmodified, consumer-grade 3D printer for the scaffold fabrication, facilitating the translation of this promising biomaterial to tissue engineering applications and promoting its wider use by the research community. Of note, the rapid prototyped PELA and HA-PELA composite scaffolds demonstrated unique swelling and mechanical properties that translated into hydration-induced self-fixation behavior. A customized specimen holder and a novel yet straightforward *in vitro* pull-out test was designed to quantify the self-fixation property resulting from hydration-induced swelling and stiffening of the amphiphilic scaffolds. The unique self-fixation behavior is attractive for scaffold-assisted tissue engineering applications where the ability of a scaffold to conform and secure itself within a tissue defect is desired for its stable implantation. We demonstrated differential abilities of rapid prototyped PELA and HA-PELA scaffolds to suppress or support the adhesion and proliferation of NIH3T3 fibroblasts and MSCs. Furthermore, MSCs adhered to HA-PELA were able to undergo potent osteogenic differentiation under *in vitro* culture induction. These cell-adhesion properties can potentially be exploited in biphasic constructs with spatially controlled cell adhesion. Future work will explore the rapid prototyped biphasic constructs for GBR where self-fixation and discrete cell adhesive properties may be exploited for facile scaffold implantation/stable fixation and promoting bone defect repair while preventing scar tissue encapsulation/soft tissue collapse.

Acknowledgments

This work was supported in part by the National Institutes of Health grants R01GM088678 and R01AR055615, and a University of Massachusetts Commercial Ventures and Intellectual Property Technology Award. Core resources supported by the National Center for Research Resources Grant S10RR021043 were used. We thank Evanthia Fylaktou and Prof. Stephen McCarthy at the University of Massachusetts Lowell for the generous help in extruding the amphiphilic polymer filaments and the kind permission for access of the extruder by Metabolix, Inc.

Disclosure Statement

No competing financial interests exist.

References

1. Faour, O., Dimitriou, R., Cousins, C.A., and Giannoudis, P.V. The use of bone graft substitutes in large cancellous voids: any specific needs? Injury **42 Suppl 2,** S87, 2011.
2. Langer, R., and Vacanti, J. Tissue engineering. Science **260,** 920, 1993.
3. Furukawa, T., *et al.* Histomorphometric study on high-strength hydroxyapatite/poly(L-lactide) composite rods for internal fixation of bone fractures. J Biomed Mater Res **50,** 410, 2000.
4. Polini, A., Pisignano, D., Parodi, M., Quarto, R., and Scaglione, S. Osteoinduction of human mesenchymal stem cells by bioactive composite scaffolds without supplemental osteogenic growth factors. PLoS One **6,** e26211, 2011.
5. Filion, T.M., *et al.* Elastomeric osteoconductive synthetic scaffolds with acquired osteoinductivity expedite the repair of critical femoral defects in rats. Tissue Eng Part A **17,** 503, 2011.
6. Filion, T.M., and Song, J. in *Biomed. Eng. - Front. Challenges* (Fazel, R.) 233–248 (InTech, 2011). doi:10.5772/22652
7. Neuendorf, R.E., Saiz, E., Tomsia, A.P., and Ritchie, R.O. Adhesion between biodegradable polymers and hydroxyapatite: relevance to synthetic bone-like materials and tissue engineering scaffolds. Acta Biomater **4,** 1288, 2008.
8. Song, J., Saiz, E., and Bertozzi, C.R. Preparation of pHEMA–CP composites with high interfacial adhesion via template-driven mineralization. J Eur Ceram Soc **23,** 2905, 2003.
9. Supová, M. Problem of hydroxyapatite dispersion in polymer matrices: a review. J Mater Sci Mater Med **20,** 1201, 2009.
10. Roach, P., Farrar, D., and Perry, C.C. Interpretation of protein adsorption: surface-induced conformational changes. J Am Chem Soc **127,** 8168, 2005.
11. Lu, D.R., and Park, K. Effect of surface hydrophobicity on the conformational changes of adsorbed fibrinogen. J Colloid Interface Sci **144,** 271, 1991.
12. Kutikov, A.B., and Song, J. An amphiphilic degradable polymer/hydroxyapatite composite with enhanced handling characteristics promotes osteogenic gene expression in bone marrow stromal cells. Acta Biomater **9,** 8354, 2013.
13. Phipps, M.C., Clem, W.C., Grunda, J.M., Clines, G.A., and Bellis, S.L. Increasing the pore sizes of bone-mimetic electrospun scaffolds comprised of polycaprolactone, collagen I and hydroxyapatite to enhance cell infiltration. Biomaterials **33,** 524, 2012.
14. Karageorgiou, V., and Kaplan, D. Porosity of 3D biomaterial scaffolds and osteogenesis. Biomaterials **26,** 5474, 2005.
15. Blakeney, B.A., *et al.* Cell infiltration and growth in a low density, uncompressed three-dimensional electrospun nanofibrous scaffold. Biomaterials **32,** 1583, 2011.
16. Leong, K.F., Cheah, C.M., and Chua, C.K. Solid freeform fabrication of three-dimensional scaffolds for engineering replacement tissues and organs. Biomaterials **24,** 2363, 2003.
17. Butscher, A., Bohner, M., Hofmann, S., Gauckler, L., and Müller, R. Structural and material approaches to bone tissue engineering in powder-based three-dimensional printing. Acta Biomater **7,** 907, 2011.
18. Sun, Y., *et al.* Degradable amorphous scaffolds with enhanced mechanical properties and homogeneous cell distribution produced by a three-dimensional fiber deposition method. J Biomed Mater Res A **100,** 2739, 2012.
19. Moroni, L., de Wijn, J.R., and van Blitterswijk, C.A. 3D fiber-deposited scaffolds for tissue engineering: influence of pores geometry and architecture on dynamic mechanical properties. Biomaterials **27,** 974, 2006.
20. Shor, L., Güçeri, S., Wen, X., Gandhi, M., and Sun, W. Fabrication of three-dimensional polycaprolactone/hydroxyapatite tissue scaffolds and osteoblast-scaffold interactions *in vitro*. Biomaterials **28,** 5291, 2007.
21. Williams, J.M., *et al.* Bone tissue engineering using polycaprolactone scaffolds fabricated via selective laser sintering. Biomaterials **26,** 4817, 2005.
22. Wiria, F.E., Leong, K.F., Chua, C.K., and Liu, Y. Poly-epsilon-caprolactone/hydroxyapatite for tissue engineering scaffold fabrication via selective laser sintering. Acta Biomater **3,** 1, 2007.
23. Schantz, J.-T., Brandwood, A., Hutmacher, D.W., Khor, H.L., and Bittner, K. Osteogenic differentiation of mesenchymal progenitor cells in computer designed fibrin-polymer-ceramic scaffolds manufactured by fused deposition modeling. J Mater Sci Mater Med **16,** 807, 2005.
24. Heo, S., *et al. In vitro* and animal study of novel nanohydroxyapatite/poly(epsilon-caprolactone) composite scaffolds fabricated by layer manufacturing process. Tissue Eng Part A **15,** 977, 2009.
25. Giordano, R.A., *et al.* Mechanical properties of dense polylactic acid structures fabricated by three dimensional printing. J Biomater Sci Polym Ed **8,** 63, 1996.
26. Kim, J., *et al.* Rapid-prototyped PLGA/β-TCP/hydroxyapatite nanocomposite scaffolds in a rabbit femoral defect model. Biofabrication **4,** 025003, 2012.
27. Woodfield, T.B.F., *et al.* Design of porous scaffolds for cartilage tissue engineering using a three-dimensional fiber-deposition technique. Biomaterials **25,** 4149, 2004.
28. Moroni, L., de Wijn, J.R., and van Blitterswijk, C.A. Three-dimensional fiber-deposited PEOT/PBT copolymer scaffolds for tissue engineering: influence of porosity, molecular network mesh size, and swelling in aqueous media on dynamic mechanical properties. J Biomed Mater Res A **75,** 957, 2005.
29. Leferink, A.M., *et al.* Increased cell seeding efficiency in bioplotted three-dimensional PEOT/PBT scaffolds. J Tissue Eng Regen Med (2013). doi:10.1002/term.1842
30. Deschamps, A.A., *et al. In vivo* and *in vitro* degradation of poly(ether ester) block copolymers based on poly(ethylene glycol) and poly(butylene terephthalate). Biomaterials **25,** 247, 2004.
31. Retzepi, M., and Donos, N. Guided bone regeneration: biological principle and therapeutic applications. Clin Oral Implants Res **21,** 567, 2010.
32. Zein, I., Hutmacher, D.W., Tan, K.C., and Teoh, S.H. Fused deposition modeling of novel scaffold architectures for tissue engineering applications. Biomaterials **23,** 1169, 2002.
33. Song, J., *et al.* Elastomeric high-mineral content hydrogel-hydroxyapatite composites for orthopedic applications. J Biomed Mater Res A **89,** 1098, 2009.
34. Cohn, D., and Younes, H. Biodegradable PEO/PLA block copolymers. J Biomed Mater Res **22,** 993, 1988.
35. Cohn, D., and Hotovely-Salomon, A. Biodegradable multiblock PEO/PLA thermoplastic elastomers: molecular design and properties. Polymer **46,** 2068, 2005.
36. Lee, J.H., Go, A.K., Oh, S.H., Lee, K.E., and Yuk, S.H. Tissue anti-adhesion potential of ibuprofen-loaded PLLA-PEG diblock copolymer films. Biomaterials **26,** 671, 2005.
37. Bedoui, F., *et al.* Anomalous increase in modulus upon hydration in random copolymers with hydrophobic segments and hydrophilic blocks. Soft Matter **8,** 2230, 2012.

38. Xu, J., Bohnsack, D.A., Mackay, M.E., and Wooley, K.L. Unusual mechanical performance of amphiphilic cross-linked polymer networks. J Am Chem Soc **129,** 506, 2007.
39. Murthy, N.S., Wang, W., and Kohn, J. Microphase separation in copolymers of hydrophilic PEG blocks and hydrophobic tyrosine-derived segments using simultaneous SAXS/WAXS/DSC. Polymer **51,** 3978, 2010.
40. Thomas, K.A., and Cook, S.D. An evaluation of variables influencing implant fixation by direct bone apposition. J Biomed Mater Res **19,** 875, 1985.
41. Verheyen, C.C., de Wijn, J.R., van Blitterswijk, C.A., de Groot, K., and Rozing, P.M. Hydroxylapatite/poly(L-lactide) composites: an animal study on push-out strengths and interface histology. J Biomed Mater Res **27,** 433, 1993.
42. Göpferich, A., Peter, S.J., Lucke, A., Lu, L., and Mikos, A.G. Modulation of marrow stromal cell function using poly(D,L-lactic acid)-block-poly(ethylene glycol)-monomethyl ether surfaces. J Biomed Mater Res **46,** 390, 1999.
43. Lieb, E., *et al.* Poly (D, L-lactic acid)-poly (ethylene glycol)-monomethyl ether diblock copolymers control adhesion and osteoblastic differentiation of marrow stromal cells. Tissue Eng **9,** 71, 2003.
44. Yang, D.-J., Chen, F., Xiong, Z.-C., Xiong, C.-D., and Wang, Y.-Z. Tissue anti-adhesion potential of biodegradable PELA electrospun membranes. Acta Biomater **5,** 2467, 2009.
45. Yang, D.-J., Xiong, C.-D., Govender, T., and Wang, Y.-Z. Preparation and drug-delivery potential of metronidazole-loaded PELA tri-block co-polymeric electrospun membranes. J Biomater Sci Polym Ed **20,** 1321, 2009.
46. Dimitriou, R., Mataliotakis, G.I., Calori, G.M., and Giannoudis, P.V. The role of barrier membranes for guided bone regeneration and restoration of large bone defects: current experimental and clinical evidence. BMC Med **10,** 81, 2012.
47. Dahlin, C., Linde, A., Gottlow, J., and Nyman, S. Healing of bone defects by guided tissue regeneration. Plast Reconstr Surg **81,** 672, 1988.
48. Melchels, F.P.W., *et al.* Effects of the architecture of tissue engineering scaffolds on cell seeding and culturing. Acta Biomater **6,** 4208, 2010.
49. Yoo, D. New paradigms in internal architecture design and freeform fabrication of tissue engineering porous scaffolds. Med Eng Phys **34,** 762, 2012.
50. Yoo, D. New paradigms in hierarchical porous scaffold design for tissue engineering. Mater Sci Eng C Mater Biol Appl **33,** 1759, 2013.
51. Kapfer, S.C., Hyde, S.T., Mecke, K., Arns, C.H., and Schröder-Turk, G.E. Minimal surface scaffold designs for tissue engineering. Biomaterials **32,** 6875, 2011.
52. Melchels, F.P.W., *et al.* Mathematically defined tissue engineering scaffold architectures prepared by stereolithography. Biomaterials **31,** 6909, 2010.

Address correspondence to:
Jie Song, PhD
Department of Orthopedics & Physical Rehabilitation
University of Massachusetts Medical School
55 Lake Ave. North
Worcester, MA 01655

E-mail: jie.song@umassmed.edu

Received: April 16, 2014
Accepted: July 10, 2014
Online Publication Date: August 19, 2014